PHYSICAL REVIEW B **91**, 085304 (2015)

Microwave magnetoplasma resonances of two-dimensional electrons in MgZnO/ZnO heterojunctions

V. E. Kozlov,[1] A. B. Van'kov,[1] S. I. Gubarev,[1] I. V. Kukushkin,[1,2] V. V. Solovyev,[1] J. Falson,[3] D. Maryenko,[4] Y. Kozuka,[3] A. Tsukazaki,[5,6] M. Kawasaki,[3,4] and J. H. Smet[2]

[1]*Institute of Solid State Physics, RAS, Chernogolovka 142432, Russia*
[2]*Max-Planck-Institut für Festkörperforschung, Heisenbergstrasse 1, D-70569 Stuttgart, Germany*
[3]*Department of Applied Physics and Quantum-Phase Electronics Center (QPEC), University of Tokyo, Tokyo 113-8656, Japan*
[4]*RIKEN Center for Emergent Matter Science (CEMS), Wako 351-0198, Japan*
[5]*Institute for Materials Research, Tohoku University, Sendai 980-8577, Japan*
[6]*PRESTO, Japan Science and Technology Agency (JST), Tokyo 102-0075, Japan*

(Received 27 June 2014; revised manuscript received 18 November 2014; published 9 February 2015)

The plasma, magnetoplasma, and edge magnetoplasma excitations were investigated in two-dimensional electron systems hosted at the heterointerface of MgZnO/ZnO structures using optical detection of resonant microwave absorption. The magnetodispersion of the plasma excitations allowed the extraction of the electron effective mass. It was found to exhibit a surprisingly large dependence on the electron density, which is difficult to account for just from nonparabolicity effects.

DOI: 10.1103/PhysRevB.91.085304 PACS number(s): 78.55.Et, 76.40.+b, 78.67.De, 71.18.+y

I. INTRODUCTION

Significant momentum has emerged in recent years around exploring the fundamental properties and potential commercial applications of wide-gap semiconductor materials. One central front is the development of optical devices which operate at blue to ultraviolet wavelengths with much effort being paid to the high quality growth of ZnSe and GaN based materials [1]. Of late, attention has expanded to oxide systems, such as ZnO and its alloys [2]. Of particular interest is Mg-doped ZnO, where by integrating an amount x of Mg into $Mg_xZn_{1-x}O$, the band gap may be tuned [3]. A fortuitous offshoot of the pursuit of growing high quality ZnO thin films has been the realization of a two-dimensional electron system (2DES) at the heterointerface of MgZnO and ZnO owing to the discontinuity in spontaneous polarization of the two layers [4]. Such heterostructures have now developed to a level of quality where the fractional quantum Hall effect is observed [5,6]. Hence, they deliver a new platform for the study of correlated electron phenomena in oxide materials.

A key parameter in any conducting system is the effective mass (m^*) of the charge carriers. It influences the mobility and important energy scales such as the Fermi and cyclotron energy. Accordingly, exploring the dependency of m^* on any adjustable parameters, for example the dielectric environment or carrier density (n_{2D}), is of paramount importance. For example, it was shown that the effective electron mass in AlGaAs/GaAs heterojunctions [7] at low temperatures shows some dependence on the energy, temperature, and n_{2D}, thereby revealing information about band nonparabolicity. In a similar vein, it has been observed in transport measurements on the MgZnO/ZnO system [8] that the electron spin susceptibility g^*m^* (where g^* is the Landé g-factor) possesses an acute dependency on n_{2D}. Quantitative experimental assessment of the systems parameters beyond transport measurements therefore remains a fitting endeavor.

In this paper we present magnetoplasma measurements on several $Mg_xZn_{1-x}O$/ZnO heterojunctions. Due to improved sample quality much more narrow and symmetric magnetoplasma resonances were observed in comparison with previous studies [9], which allows the exploration of how m^* of the charge carriers in the MgZnO/ZnO 2DES changes with n_{2D}. The magnetodispersion behavior of the upper magnetoplasma branch enables us to extract its value and reveals a steady enhancement when increasing n_{2D}. We consider that nonparabolicity of the conduction band alone cannot explain this tendency and therefore propose a nonparabolicity mediated circumvention of Kohn's theorem in the presence of strong Coulomb interactions as a possible explanation.

II. EXPERIMENTAL TECHNIQUE

The experiments reported here have been performed on a set of six heterostructures containing a single $Mg_xZn_{1-x}O$/ZnO heterojunction and covering electron densities from 0.7 to $11 \times 10^{11}/cm^2$. These densities were determined from Shubnikov–de Haas oscillations in transport as well as magneto-oscillations in the photoluminescence intensity [10,11]. Low temperature measurements between 0.3 and 3 K and magnetic fields up to 14 T were carried out by mounting the sample in a ^{3}He sample holder of a bath cryostat. Photoluminescence spectra were recorded by exciting the sample with a continuous-wave He-Cd laser with a wavelength of 325 nm. The maximum optical power delivered to the sample was approximately 20 $\mu W/mm^2$. The spectra were recorded with the help of a nitrogen-cooled CCD matrix and a Monospec spectrometer with a linear dispersion of 5 Å/mm and a spectral resolution of 0.3 Å.

To detect magnetoplasma excitations with frequencies up to 28 GHz, the samples were placed in an SMA connector at the end of a coaxial cable guiding the microwave excitation from a generator down to the center of the magnet of the bath cryostat. This arrangement offers a nearly flat response to excitation frequencies ranging from 0.1 up to 28 GHz. To detect magnetoplasmons luminescence spectra with and without microwave excitation were recorded consecutively. If the incident microwave radiation is in resonance with a plasma

excitation, the electronic system will heat up due to the absorption of microwave power. The redistribution of electrons across the energy spectrum, induced by the temperature increase, will cause modifications in the luminescence spectrum. These can be made visible by subtracting the spectrum in the absence of microwave irradiation from the spectrum acquired under microwave excitation. The microwave absorption amplitude is then defined as the integral of the absolute value of this differential luminescence spectrum over the measured spectral range. To detect a resonance either the microwave frequency is swept at a fixed magnetic field or the magnetic field is ramped at a fixed excitation frequency. To investigate resonances above 28 GHz the sample is mounted near the end of an oversized microwave waveguide. This arrangement does not offer a flat frequency response and hence is only suitable for magnetic field scans. The excellent sensitivity of this technique, referred to as optical detection of resonant microwave absorption (ODRMA), has been established previously [12,13].

III. TWO-DIMENSIONAL NATURE OF THE PHOTOLUMINESCENCE SIGNAL

Figure 1 displays an example of photoluminescence spectra recorded in the absence and presence of microwave radiation on a $Mg_{0.045}Zn_{0.955}O/ZnO$ single heterointerface at zero magnetic field. Also shown is their differential spectrum. The photoluminescence signal at energies between 3.363 and 3.366 eV is absent in bulk ZnO samples and is therefore attributed to the two-dimensional electronic system (2DES) formed close to the heterointerface. The signal consists of a broad, asymmetric line and spans roughly 3 meV. It has been demarcated by two dashed lines marked as the bottom of the lowest subband E_0 and $E_0 + E_F$, where E_F is the chemical potential. Corroborating evidence for the two-dimensional nature of this photoluminescence signal comes from data acquired in a magnetic field.

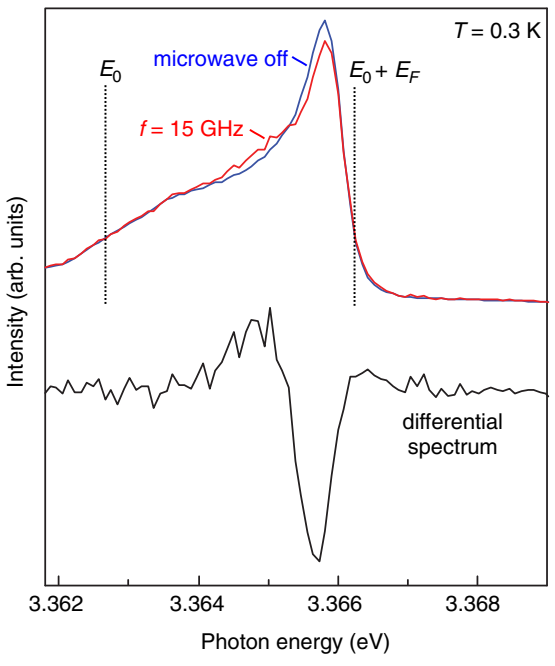

FIG. 1. (Color) Luminescence spectrum at zero magnetic field of the 2DES formed at a $Mg_{0.045}Zn_{0.955}O/ZnO$ heterojunction with an electron density of $n_{2D} = (6.54 \pm 0.03) \times 10^{11}$ cm^{-2} in the presence (red line) and absence (blue line) of microwaves with a frequency of 15 GHz. The sample had a rectangular shape with a length a of 1.85 mm and a width b of 1.15 mm. The black line is the differential spectrum. Features between E_0 and $E_0 + E_F$ stem from the recombination of electrons from the lowest subband.

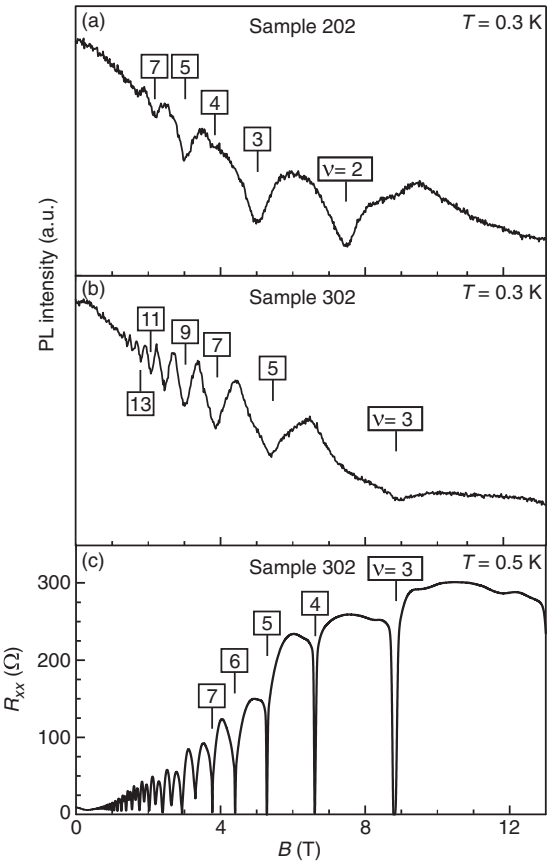

FIG. 2. The magnetic field dependence of the photoluminescence intensity measured for sample 202 (a) and sample 302 (b) at a fixed photon energy 3.366 eV, corresponding to the position of the chemical potential. Several minima at integer filling factors are marked. The 2D-electron density was calculated from these minima as 3.66×10^{11} cm^{-2} for sample 202 and 6.54×10^{11} cm^{-2} for sample 302. (c) The Shubnikov–de Haas oscillations measured for sample 302. They yield a 2D-electron density $n_{2D} = 6.1 \times 10^{11}$ cm^{-2} and mobility $\mu = 2 \times 10^5$ cm^2/V s.

Figures 2(a) and 2(b) display the intensity of the photoluminescence signal for two samples of different density (samples 202 and 302) as a function of the magnetic field at a fixed energy of 3.366 eV. They exhibit a series of oscillations. These oscillations are periodic when plotted on a $1/B$ axis. The location of each minimum is insensitive to the in-plane component of the magnetic field when tilting the sample. These observations confirm the two-dimensional character of the electrons involved in the photoluminescence recombination. The observed oscillation minima correspond to integer filling of the Landau levels [14] and the periodicity allows us to extract the 2D-electron density n_{2D}. Because in ZnO the Zeeman energy is comparable in size with

the cyclotron energy, Landau levels with the same index but opposite spin are further apart compared with adjacent Landau levels of opposite spin. As a result odd filling factors are resolved first. For sample 202 in Fig. 2(a) one obtains $n_{2D} = (3.66) \times 10^{11}$ cm^{-2}. For sample 302 in Fig. 2(b) we get $n_{2D} = (6.54 \pm 0.03) \times 10^{11}$ cm^{-2}. Figure 2(c) plots the Shubnikov–de Haas oscillations from a magnetotransport experiment for this sample. The electron density agrees within 6% of the value extracted from luminescence. This small discrepancy may be the result of sample inhomogeneity, since transport and optical data were obtained from two different pieces of the wafer. The photoconductivity effect, which may cause a density difference in optical experiments is—in contrast with modulation doped GaAs based 2D electron systems [15]—weak. The electron density hardly changed with power and no evidence for persistent parallel conductivity was observed in transport under illumination.

IV. OPTICAL DETECTION OF RESONANT MICROWAVE ABSORPTION

By measuring differential luminescence spectra, as plotted in Fig. 1, at different values of the magnetic field and microwave frequency and by evaluating the microwave absorption strength when building the integral of these differential spectra across the measured spectral range, it is possible to detect magnetoplasma excitations. For illustrative purposes such resonances in the microwave absorption amplitude are plotted in Figs. 3(a) and 3(b) for samples 202 and 302, respectively. The microwave frequency is swept and the magnetic field B serves as a discrete parameter. At low magnetic field only one absorption resonance is observed. The resonance frequency decreases with increasing magnetic field. This negative dispersion with magnetic field is characteristic of edge magnetoplasmon excitations in 2DES [13,16]. The linewidth of the plasma resonance enables us to extract the momentum relaxation time of the 2D electrons. For all measured samples this time varied from 30 to 50 ps, values in good agreement with momentum relaxation times extracted from transport data.

To detect resonances at frequencies exceeding 28 GHz the samples were mounted in an oversized waveguide, which does not offer a flat frequency response. Hence, resonances need to be detected by sweeping the magnetic field as illustrated in Fig. 4. Now, the resonance shifts with increasing microwave frequency to higher magnetic fields. This positive magnetodispersion is a characteristic feature of bulk magnetoplasmons [13,16]. The positions of all resonances observed up to 65 GHz for sample 202 are compiled in Fig. 5(a). The bulk magnetoplasmons with positive magnetodispersion and the edge magnetoplasmons with negative magnetodispersion can easily be distinguished in this representation of the data.

In the remainder of this section we analyze the dispersion of these magnetoplasmon excitations. In rectangular samples with side lengths a and b in the x and y direction, respectively, the frequencies of the plasmons propagating in the x or y direction in the absence of an external magnetic field can be

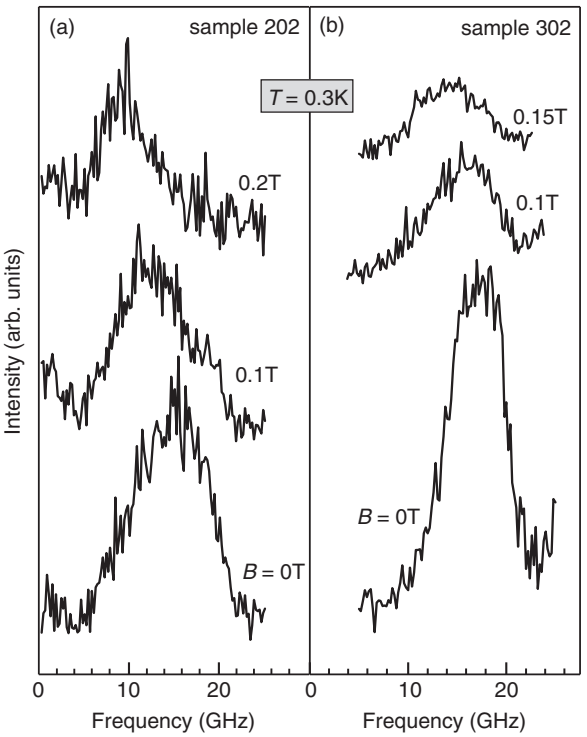

FIG. 3. Optically detected resonant microwave absorption measurements carried out on two samples. The microwave absorption amplitude is plotted as a function of the incident microwave frequency for three different values of the perpendicular magnetic field. In (a) the resonances recorded on sample 202 with a density of $n_{2D} = 3.66 \times 10^{11}$ cm^{-2} are plotted. (b) The results on sample 302 with $n_{2D} = 6.54 \times 10^{11}$ cm^{-2}.

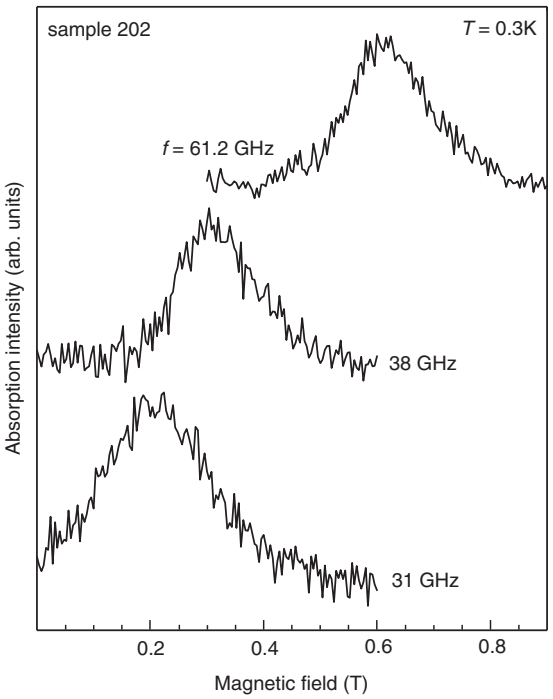

FIG. 4. The microwave absorption amplitude recorded on sample 202 as a function of the magnetic field for microwave frequencies beyond 28 GHz. The resonances correspond to the bulk magnetoplasma mode with positive magnetic field dispersion.

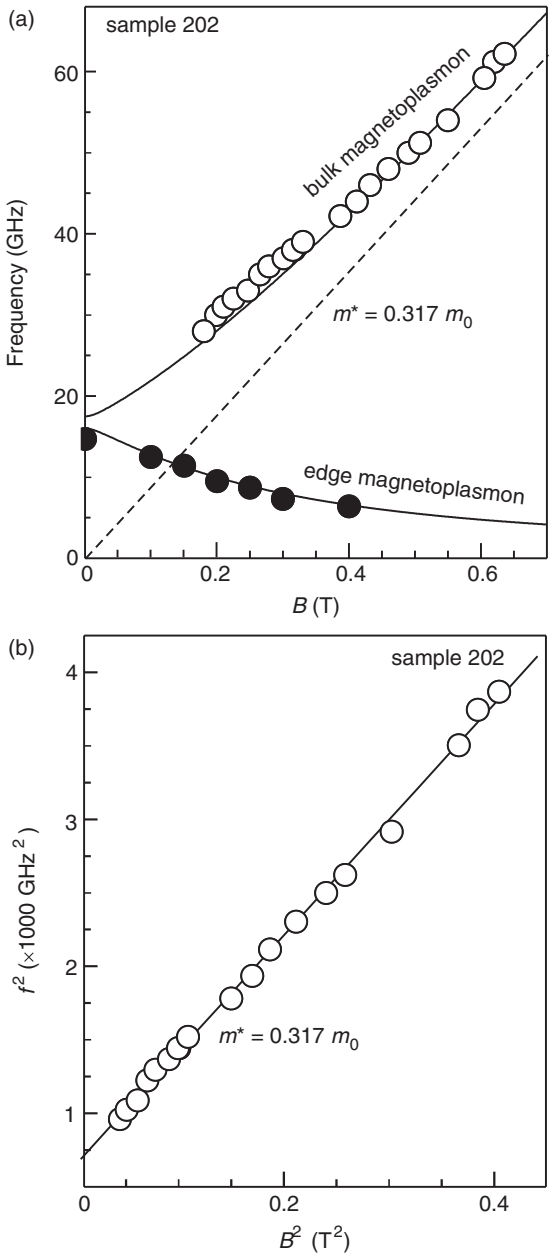

FIG. 5. Frequencies of the magnetoplasma resonances versus perpendicular magnetic field for sample 202. (a) Solid bullets (•) correspond to the resonances obtained from frequency scans from 0 to 28 GHz measured at fixed magnetic fields. These resonances form the lower edge magnetoplasma mode. Open bullets (○) correspond to the resonances obtained from magnetic field scans at fixed frequencies exceeding 28 GHz. The data points describe the bulk magnetoplasma mode. The solid lines represent the theoretical dependencies given by Eq. (3). The dashed line is the cyclotron frequency eB/m^*. (b) The bulk magnetoplasma branch of sample 202 in (a) is replotted using B^2 as abscissa and f^2 as the ordinate. The data points fall on a line whose slope yields an accurate value of the effective mass.

written as

$$\omega_x^2 = \frac{n_{2D}e^2}{2m^*\bar{\varepsilon}}q_x, \tag{1}$$

$$\omega_y^2 = \frac{n_{2D}e^2}{2m^*\bar{\varepsilon}}q_y. \tag{2}$$

TABLE I. Overview of the key parameters of the six samples investigated in this study: charge carrier density n_{2D} and side lengths a and b.

Sample	n_{2D} (10^{11} cm^{-2})	a (mm)	b (mm)
080	0.7	6	6
232	1.7	6	6
244	2.2	6	6
202	3.7	1.1	0.9
302	6.5	1.85	1.15
431	11	0.7	0.7

Here $\bar{\varepsilon} = (8.5 + 1)/2\varepsilon_0 = 4.75\varepsilon_0$ is the dielectric constant of the half space, and $q_x = \pi/a$ and $q_y = \pi/b$ are the wave vector components for the fundamental plasmon modes [13]. From these expressions it follows that differences in sample size should cause a noticeable difference in the plasma frequencies. Table I summarizes the side lengths for the six different samples used in these investigations.

The dispersion of the plasma excitations in a magnetic field is caused by a hybridization of the different plasma modes with the cyclotron mode. To describe the coupling between the cyclotron and plasma modes we use the expressions from Ref. [17] derived for elliptically shaped disks as an approximation, since for rectangular shaped samples no analytical expressions exists. The spectrum for elliptical shaped disks is also determined by the two plasma frequencies ω_x and ω_y:

$$\omega_\pm^2 = \left(\omega_x^2 + \omega_y^2 + \omega_c^2\right)/2 \pm \left\{\left(\omega_x^2 + \omega_y^2 + \omega_c^2\right)^2/4 - \omega_x^2\omega_y^2\right\}^{1/2}. \tag{3}$$

Here ω_c is the cyclotron frequency and equals eB/m^*. These expressions correctly describe the splitting at zero magnetic field and also the dispersion of the magnetoplasma modes at high magnetic fields. The frequency of the upper magnetoplasma mode asymptotically approaches the cyclotron energy and the lower mode frequency decreases with the B field as $\sim 1/B$.

The solid lines in Fig. 5 are best fits to the data using the effective mass as a fit parameter in Eq. (3). These fits agree well with the experimental data and correctly capture both magnetoplasma branches. The value of the electron effective mass can be more accurately extracted from the magnetodispersion of the bulk magnetoplasma mode considering its asymptotic behavior at high magnetic fields:

$$\omega^2 = A + \omega_c^2, \tag{4}$$

where A is a constant shift due to the zero field plasma frequency, which depends on the sample geometry. As an example, the data points forming the bulk magnetoplasma branch in sample 202 are replotted in Fig. 5(b) using f^2 as the ordinate and B^2 as abscissa. The slope of the observed dependence enables an accurate calculation of the electron effective mass.

The five other samples, whose parameters are summarized in Table I, were analyzed in the same manner. Figure 6 plots the extracted value of the effective mass m^* for all measured samples as a function of the charge carrier density. A significant increase is observed at all densities compared with the effective

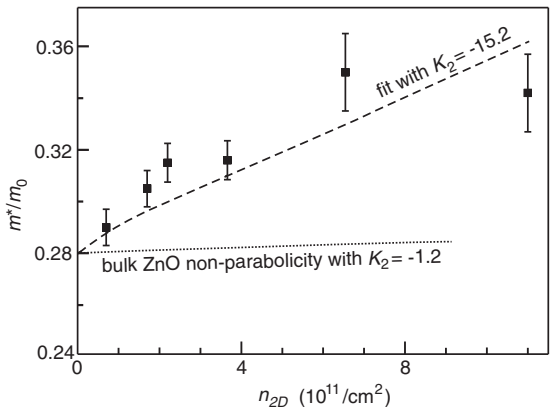

FIG. 6. The electron effective mass m^* as a function of the electron density for the six $Mg_xZn_{1-x}O$/ZnO heterojunctions listed in Table I. Symbols: Experimental values extracted from a fit to the magnetic field dependence of the magnetoplasmon excitations. Dotted curve is a calculated mass dependence with the nonparabolicity parameter $K_2^{\rm bulk} = -1.2$, extracted from the data for bulk ZnO [19]. The dashed curve is the theoretical dependence described by Eq. (6) for a value of K_2 equal to -15.2.

mass at low density. A specific functional dependence cannot be derived, but a rough linear approximation is possible up to 6.54×10^{11} cm^{-2}, while the higher density point suggests a saturation.

V. DISCUSSION

An increase of the cyclotron effective mass with density in a 2DES in a polar semiconductor is generally attributed to interband coupling (or nonparabolicity) or electron-phonon coupling effects (polaron coupling). A similar experimental study of the cyclotron effective mass as a function of the carrier density has been conducted on AlGaAs/GaAs heterojunctions [7]. This study was performed in a comparable range of densities up to $n_{2D} \sim 9 \times 10^{11}$ cm^{-2}. The authors were able to describe the linear growth of the cyclotron effective mass using a $\vec{k} \cdot \vec{p}$ model including three bands. Within this three band model, the dispersion of the conduction band can be written as

$$E(k) = \frac{\hbar^2 k^2}{2m^*} + \frac{K_2}{E_g}\left(\frac{\hbar^2 k^2}{2m^*}\right)^2. \quad (5)$$

Here K_2 is a coefficient controlling the size of the energy dependent nonparabolicity and E_g is the fundamental band gap. The behavior of the effective mass with energy is given by

$$\frac{1}{m^*(E)} = \frac{1}{m_0^*}\left(1 + \frac{2K_2}{E_g}E\right). \quad (6)$$

In this expression, m_0^* is the band-edge effective mass and E is the energy of the electrons. For GaAs the value of K_2 was estimated to be -1.4. It is important to note that in GaAs-based structures, cyclotron resonance data obtained in the low magnetic field limit are not subject to polaron coupling effects as long as the cyclotron energy is substantially smaller than the LO-phonon energy. The data for ZnO heterostructures in Figs. 5 and 6 have been analyzed analogously. Polaron coupling should be even less significant in ZnO, since the LO-phonon energy is larger than in GaAs, $\hbar\omega_{\rm LO}^{\rm ZnO} = 72$ meV, and the cyclotron energy is substantially reduced. At the applied magnetic fields for all data points in Fig. 6, $\hbar\omega_c$ is smaller than 0.4 meV.

In quasi-2D electron systems formed at heterojunctions, the energy E of electrons at the chemical potential or Fermi energy in the limit of zero temperature is composed of two contributions: the kinetic energy associated with the in-plane motion E_F, and the confinement energy E_z due to the finite extent of the wave function in the z direction. Both depend strongly on the electron density. It is possible to estimate E_z from the Fang and Howard [18] variational wave function $\phi(z)$ for the first subband of an inversion charge layer:

$$\phi(z) = \left(\frac{c^3}{2}\right)^{1/2} z\, e^{-cz/2}. \quad (7)$$

Here $c = [12m_z e^2(n_{\rm dep} + 11/32 n_{2D})/\varepsilon_{\rm ZnO}\hbar^2]^{1/3}$. For MgZnO/ZnO heterostructures we take the following parameters: $\varepsilon_{\rm ZnO} = 8.5\varepsilon_0$, $m_z = 0.3m_0$, $n_{\rm dep} = 0$. The confinement energy takes on the value

$$E_z = \frac{\hbar^2 c^2}{8m_z}. \quad (8)$$

For the above parameters one may simulate the effective mass dependence on the carrier density by calculating the total energy of the electrons at the Fermi level and substituting this energy E into Eq. (6). The carrier density dependence of both terms contributing to E are given by $E_z = n_{2D}^{2/3} \cdot 3.37$ meV and $E_F = n_{2D} \cdot 0.795$ meV, where n_{2D} is taken in units of 10^{11} cm^{-2}. The best fit of the resulting expression to the experimental data is shown in Fig. 6 as the dashed curve and yields a value of the nonparabolicity coefficient K_2 equal to -15.2. The lowest estimate of K_2 is no less than -12. Although there is some scatter in the data and the dependence of the experimental mass does only roughly obey the trend predicted by this theoretical expression, it is obvious that all estimated K_2 values are an order of magnitude larger than in GaAs. This large nonparabolicity coefficient is surprising, since the nonparabolicity effect in wide-band-gap wurtzite semiconductors is usually smaller relative to most zinc-blende compounds [19]. Indeed, nonparabolicity coefficients obtained for bulk ZnO in Ref. [19] by a best fit to dichroism and ellipsometry data yield $K_2^{\rm bulk} \sim -1.2$ (see dotted line in Fig. 6).

It is plausible to conclude that interband coupling is not the only mechanism responsible for the observed drastic increase of the electron effective mass with charge carrier density in the ZnO 2D system. Coulomb correlations are likely to play an important role in this material. The key parameter here is the ratio of the Coulomb energy scale and the kinetic energy. This ratio or r_s parameter is approximately 7 times larger in ZnO compared with GaAs. The combined influence of nonparabolicity and Coulomb correlations on the cyclotron resonance energy in 2D electron systems was considered in a theoretical study by MacDonald and Kallin [20]. It was established that, given strong Coulomb correlations in the system, even weak nonparabolicity effects can substantially shift the energy of the cyclotron resonance, transform it into

a collective excitation, and cause other anomalies in the cyclotron resonance spectrum. Due to the nonparabolicity Kohn's theorem is not valid and Coulomb correlations do affect the cyclotron resonance even if we probe the system in the limit of zero momentum. We speculate that the strong increase of the effective mass with electron density is a qualitative manifestation of this Coulomb contribution to the cyclotron resonance energy.

Additional evidence that Coulomb correlations do modify the effective mass of the quasiparticles in the conduction band stems from the photoluminescence recombination line in Fig. 1. The average effective mass can be extracted from the energy spanned by this line ($E_F \sim 3.4$ meV). This yields $m^* = \pi\hbar^2 n_s / E_F \approx 0.45\, m_0$. This effective mass can be considered as an interaction-renormalized mass of the Fermi-liquid quasiparticles. Its value is 50% larger in comparison with the value extracted from the cyclotron resonance data.

In conclusion, the radiative recombination of 2D electrons with photoexcited holes has been studied in MgZnO/ZnO heterojunctions for magnetic fields up to 14 T. Bulk and edge magnetoplasmon excitations were observed using the optical detection of resonant microwave absorption. The cyclotron mass extracted from these experiments exhibits a strong dependence on electron density. Nonparabolicity effects in conjunction with strong Coulomb interactions are held responsible for this density dependence.

ACKNOWLEDGMENTS

I.V.K., A.B.V., V.E.K., S.I.G., and V.V.S. thank the Russian Scientific Foundation (Grant No. 14-12-00693) for support in developing the method of optical detection of resonant microwave absorption in ZnO heterostructures. This work was partly supported by Grant-in-Aids for Scientific Research (S) No. 24226002 from MEXT, Japan, "Funding Program for World-Leading Innovative R&D on Science and Technology (FIRST)," Program from the Japan Society for the Promotion of Science (JSPS) initiated by the Council for Science and Technology Policy. J.F. acknowledges the support of the Marubun Research Promotion Foundation.

[1] H. Morkoç, *Handbook of Nitride Semiconductors and Devices: GaN-based Optical and Electronic Devices* (Wiley, Weinheim, 2009), Vol. 3.

[2] Y. Kozuka, A. Tsukazaki, and M. Kawasaki, Appl. Phys. Rev. **1**, 011303 (2014).

[3] A. Ohtomo, M. Kawasaki, T. Koida, K. Masabuchi, H. Koinuma, Y. Sakurai, Y. Yoshida, T. Yasuda, and Y. Segawa, Appl. Phys. Lett. **72**, 2466 (1998).

[4] J. Falson, D. Maryenko, Y. Kozuka, A. Tsukazaki, and M. Kawasaki, Appl. Phys. Express **4**, 091101 (2011).

[5] A. Tsukazaki, S. Akasaka, K. Nakahara, Y. Ohno, H. Ohno, D. Maryenko, A. Ohtomo, and M. Kawasaki, Nat. Mater. **9**, 889 (2010).

[6] D. Maryenko, J. Falson, Y. Kozuka, A. Tsukazaki, M. Onoda, H. Aoki, and M. Kawasaki, Phys. Rev. Lett. **108**, 186803 (2012).

[7] M. A. Hopkins, R. J. Nicholas, M. A. Brummell, J. J. Harris, and C. T. Foxon, Phys. Rev. B. **36**, 4789 (1987).

[8] Y. Kozuka, A. Tsukazaki, D. Maryenko, J. Falson, C. Bell, M. Kim, Y. Hikita, H. Y. Hwang, and M. Kawasaki, Phys. Rev. B **85**, 075302 (2012).

[9] Y. Kasahara, Y. Oshima, J. Falson, Y. Kozuka, A. Tsukazaki, M. Kawasaki, and Y. Iwasa, Phys. Rev. Lett. **109**, 246401 (2012).

[10] V. E. Kozlov, A. B. Van'kov, S. I. Gubarev, I. V. Kukushkin, J. Falson, D. Maryenko, Y. Kozuka, A. Tsukazaki, M. Kawasaki, and J. H. Smet, JETP Letters **98**, 223 (2013).

[11] T. Makino, Y. Segawa, A. Tsukazaki, H. Saito, S. Takeyama, S. Akasaka, K. Nakahara, and M. Kawasaki, Phys. Rev. B **87**, 085312 (2013).

[12] I. V. Kukushkin, J. H. Smet, K. von Klitzing, and W. Wegscheider, Nature (London) **415**, 409 (2002).

[13] I. V. Kukushkin, J. H. Smet, S. A. Mikhailov, D. V. Kulakovskii, K. von Klitzing, and W. Wegscheider, Phys. Rev. Lett. **90**, 156801 (2003).

[14] I. V. Kukushkin and V. B. Timofeev, Adv. Phys. **45**, 147 (1996).

[15] S. Luryi and A. Kastalsky, Appl. Phys. Lett. **45**, 164 (1984).

[16] V. A. Volkov and S. A. Mikhailov, in *Landau Level Spectroscopy*, edited by G. Landwehr and E. I. Rashba, Modern Problems in Condensed Matter Sciences, Vol. 27.2 (North-Holland, Amsterdam, 1991), Chap. 15, p. 855.

[17] C. Dahl, F. Brinkop, A. Wixforth, J. P. Kotthaus, J. H. English, and M. Sundaram, Solid State Commun. **80**, 673 (1991).

[18] F. F. Fang and W. E. Howard, Phys. Rev. Lett. **16**, 797 (1966).

[19] S. Shokhovets, O. Ambacher, B. K. Meyer, and G. Gobsch, Phys. Rev. B **78**, 035207 (2008).

[20] A. H. MacDonald and C. Kallin, Phys. Rev. B **40**, 5795 (1989).